Title

Calibration between trigger and color: Neutralization of a genetically encoded coulombic switch and dynamic arrest precisely tune reflectin assembly

Journal

Journal of Biological Chemistry, 294(45)

ISSN

0021-9258

Authors

Levenson, Robert
Bracken, Colton
Sharma, Cristian
et al.

Publication Date

2019-11-01

DOI

10.1074/jbc.ra119.010339

Peer reviewed

Calibration between trigger and color: Neutralization of a genetically encoded coulombic switch and dynamic arrest precisely tune reflectin assembly

Received for publication, July 31, 2019, and in revised form, September 14, 2019 Published, Papers in Press, September 26, 2019, DOI 10.1074/jbc.RA119.010339

Robert Levenson, Colton Bracken, Cristian Sharma, Jerome Santos, Claire Arata, Brandon Malady, and Daniel E. Morse[1]

From the Department of Molecular, Cellular and Developmental Biology and the Institute for Collaborative Biotechnologies, University of California, Santa Barbara, California 93106-5100

Edited by Joseph M. Jez

Reflectin proteins are widely distributed in reflective structures in cephalopods. However, only in loliginid squids are they and the subwavelength photonic structures they control dynamically tunable, driving changes in skin color for camouflage and communication. The reflectins are block copolymers with repeated canonical domains interspersed with cationic linkers. Neurotransmitter-activated signal transduction culminates in catalytic phosphorylation of the tunable reflectins' cationic linkers; the resulting charge neutralization overcomes coulombic repulsion to progressively allow condensation, folding, and assembly into multimeric spheres of tunable well-defined size and low polydispersity. Here, we used dynamic light scattering, transmission EM, CD, atomic force microscopy, and fluorimetry to analyze the structural transitions of reflectins A1 and A2. We also analyzed the assembly behavior of phosphomimetic, deletion, and other mutants in conjunction with pH titration as an *in vitro* surrogate of phosphorylation. Our experiments uncovered a previously unsuspected, precisely predictive relationship between the extent of neutralization of a reflectin's net charge density and the size of resulting multimeric protein assemblies of narrow polydispersity. Comparisons of mutants revealed that this sensitivity to neutralization resides in the linkers and is spatially distributed along the protein. Imaging of large particles and analysis of sequence composition suggested that assembly may proceed through a dynamically arrested liquid–liquid phase-separated intermediate. Intriguingly, it is this dynamic arrest that enables the observed fine-tuning by charge and the resulting calibration between neuronal trigger and color in the squid. These results offer insights into the basis of reflectin-based biophotonics, opening paths for the design of new materials with tunable properties.

Cephalopods such as squid and octopuses possess an optically dynamic epithelium, enabling complex camouflage and communication (1, 2). In addition to pigmentary chromatophores, these animals possess reflective cells, leucophores and iridocytes, that act as structural reflectors through the interaction of light with their subwavelength nanostructures (3, 4). Although leucophores are broadband scatterers of white light, iridocytes reflect specifically colored, iridescent light by angle- and wavelength-dependent constructive interference from intracellular Bragg reflectors. The lamellae of these reflectors are densely filled with cationic block copolymer-like proteins called reflectins and are separated from the low-refractive-index extracellular fluid by regular invaginations of the cell membrane (5–9).

Although the structural reflectors of the iridocytes and leucophores of most cephalopods are static, those in the Loliginidae squid family uniquely possess reversibly tunable versions of these reflectors (10). Ultrastructural characterization of unactivated tunable iridocytes showed their intracellular lamellae to contain a heterogeneous mixture of discontinuous ~10–20-nm nanoparticles and nanofibrils, suggesting that the cationic reflectins within exist in a predominantly unassembled state dominated by interparticle charge repulsion (10, 11). However, upon iridocyte activation initiated by binding of the neurotransmitter acetylcholine, released from nearby nerve cells, to cell-surface muscarinic receptors, a signal transduction cascade culminates in enzymatic phosphorylation of the reflectins, consequently neutralizing their cationic charge and driving assembly of the reflectins to form homogenous densely staining Bragg lamellae (6, 8, 11, 12). Measurements demonstrating the reversible efflux of D_2O and its reuptake revealed that condensation of the reflectins drives the expulsion of H_2O from the membrane-bounded lamellae, simultaneously increasing the refractive index contrast between the intracellular and extracellular layers of the Bragg reflector while shrinking their thickness and spacing, thus activating reflectance and progressively tuning the color of the reflected light across the visible spectrum (7, 8, 13, 14).

The role of the reflectins as tunable drivers of this biophotonic behavior has generated interest in understanding the principles underlying their responsiveness to signal-activated phosphorylation and their resulting changes in conformation and assembly. The reflectins are essentially block copolymers, composed of highly conserved reflectin domains ("reflectin

This work was supported by United States Department of Energy, Basic Energy Sciences Grant DE-SC0015472; the Institute for Collaborative Biotechnologies through Grant W911NF-09-0001 from the United States Army Research Office; and Army Research Office Grant W911NF-17-1-0160. The authors declare that they have no conflicts of interest with the contents of this article.

This article contains Figs. S1–S9.

[1] To whom correspondence should be addressed. E-mail: d_morse@lifesci.ucsb.edu.

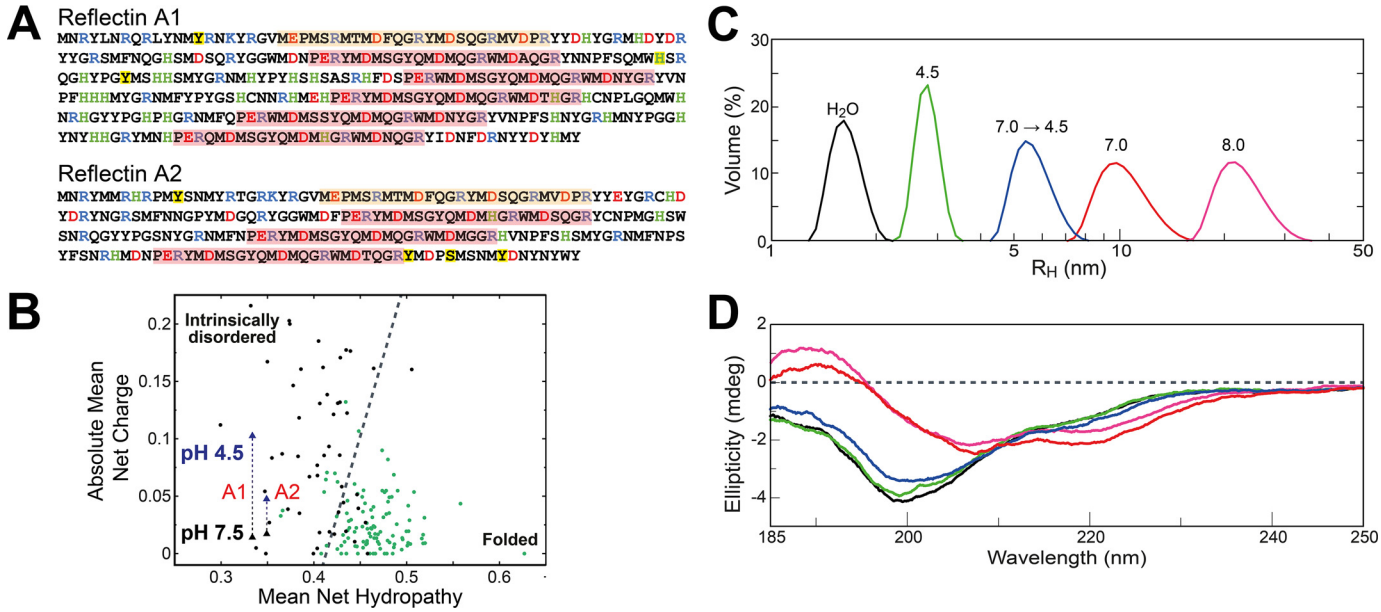

Figure 1. *A*, sequences of *D. opalescens* reflectins A1 and A2. Conserved N-terminal domains are highlighted with *dark yellow*; other repeat domains are highlighted with *pale red*. Histidine residues are *green*, other positively charged residues are *blue*, negatively charged residues are *bright red*, and phosphorylation sites are highlighted with *bright yellow*. *B*, absolute mean net charge *versus* hydropathy of a previously determined library of proteins (*circles*) and the reflectins (*triangles*). *Black triangles* designate mean net charge at neutral pH where histidine residues are neutralized; *blue triangles* designate acidic pH conditions where histidines are presumed uniformly charged. In all other reference proteins, histidines are considered neutral. Mean hydropathy was calculated using the Kyte–Doolittle scale (54). *C*, DLS of A1 WT monomers (H_2O and pH 4.5; *black* and *green*, respectively), multimers (pH 7.0; *red*), and oligomers (reversed from pH 7.0 to 4.5; *blue*) as labeled in the panel. Minority (generally <5% of total reflectin chain volume/mass) populations of substantially larger aggregates, seen previously and by other methods described in this work, are excluded from this panel for clarity (16). Data are depicted as the volume distribution, which is directly proportional to the mass of reflectin and compensates for the exponentially greater scattering intensity of larger particles. *D*, CD spectra of A1 in monomeric, oligomeric, and multimeric states. *Line colors* correspond to conditions as labeled in the previous panel. *mdeg*, millidegrees.

motifs" (RMs))[2] interspersed with cationic linkers, as seen for reflectins A1 and A2 of the loliginid squid *Doryteuthis opalescens* (see Fig. 1*A*). The reflectins exhibit a unique amino acid composition with some heterogeneity across their sequences; they are highly enriched in methionine, arginine, and tyrosine residues but possess almost no (<1%) aliphatic residues (5, 9, 10). The sequence composition of the reflectins suggests that attractive interactions are likely to be primarily driven by tyrosine–aromatic (π–π), arginine–tyrosine (cation–π), and methionine–tyrosine (sulfur–π) interactions, forming a complex interaction network of both intra- and interstrand noncovalent bonding (10, 15).

Recently, we demonstrated an *in vitro* assay that examined the assembly of purified recombinant *D. opalescens* reflectins as a function of progressive neutralization, as a surrogate of *in vivo* phosphorylation, through dilution of the H_2O-solubilized proteins into low-ionic-strength buffers of varying pH (16). Analyzing the tunable reflectins and a variety of mutant derivatives, we now show *in vitro* a predictive relationship between the extent of charge neutralization of the positively charged linker peptides and the size of the resulting assembled reflectin multimers. This discovery further elucidates the mechanistic origin of the synergistic effects of reflectin neutralization on the color and brightness of light reflected *in vivo*. Mutational analyses reveal that the "switch" controlling the neutralization-dependent structural transitions underlying tunability is not localized but instead is spatially distributed in the multiple linkers along the reflectin's length.

[2] The abbreviations used are: RM, reflectin motif; DLS, dynamic light scattering; TEM, transmission EM; AFM, atomic force microscopy; L, linker; LLPS, liquid–liquid phase segregation.

Results

Bioinformatics analyses suggests that the reflectins are intrinsically disordered

The tunable reflectins from the loliginid squid *D. opalescens* are essentially block-copolymeric, composed of unique and highly conserved peptide domains alternating with weakly polycationic linkers (Figs. 1*A* and S1A) (10). Secondary structure algorithms do not predict significant α or β structure, indicating that the reflectins are intrinsically disordered (5, 6). Comparison of *D. opalescens* reflectins A1 and A2 overall net charge and mean hydropathy with those of a collection of proteins previously analyzed for structure shows that these two sequence parameters are in the range commonly observed for intrinsically disordered proteins (Fig. 1*B*) (17). Use of the FoldIndex tool, which performs this same calculation using a moving window across the protein sequence, yields uniform scores across the entire reflectin A1 and A2 sequences, indicating that the conserved domains and linkers do not vary in their drive to fold when analyzed in their unmodified, native state (Fig. S1, A and B). Use of the meta-predictors PONDR-FIT and MetaDisorder support this assessment, assigning either disordered or borderline-ordered scores that show no correlation with conserved domain or linker sequences (Fig. S1, C and D). These bioinformatics analyses agree with previous experimental analyses of reflectin nanoparticles by X-ray scattering, circular dichroism (CD), and FTIR spectroscopy as well as the CD anal-

yses discussed below, all indicating that unmodified reflectins are largely disordered (7, 18–21). Interestingly, *D. opalescens* reflectins A1 and A2 show overall greater predicted levels of intrinsic disorder than reflectins from other cephalopod species, which do not display tunable iridescence (Fig. S1, C and D) (10). This marginally greater drive of the *D. opalescens* reflectins toward disorder encoded within their sequences may play a role in enabling tunable assembly by shifting the equilibrium *in vivo* between the monomeric and assembled states, favoring disassembly in the absence of a triggering stimulus (10). In contrast with these differences, reflectins from tunable and non-tunable species show no significant differences in hydropathy (Fig. S1E).

Initially unstructured monomeric reflectin reversibly forms nanoparticles of well-defined size

Dynamic light scattering (DLS) of 9 μM purified recombinant reflectin A1 wildtype (WT) in H_2O-solubilized (pH 3.5) or buffered acidic pH 4.5 conditions measures particles consistent with monomeric states (Fig. 1*C*). Dilution of H_2O-solubilized monomer into buffers at pH ≥6.5 drives reversible assembly of spherical nanoparticle multimers of tunable size, estimated to contain tens to thousands of reflectin monomers. Sizes estimated by DLS were previously found to agree closely with those measured by transmission EM (TEM) (16). Following neutralization and assembly of the reflectins, minority populations of larger aggregates (typically <5–10% of total reflectin mass as indicated by DLS volume distributions) often were observed in addition to the majority population of predicted assemblies, consistent with our findings by TEM described below and our previous observations (16). This neutralization-driven assembly can be reversed by acidification with low concentrations of acetic acid, driving disassembly to form particles with R_H values of ~6 nm. These particles can be cycled back to a multimeric state by dialysis into higher-pH buffer as shown previously (16).

CD spectra of monomeric *D. opalescens* A1 WT in both H_2O-solubilized and acidic pH 4.5 conditions show strong minima near 200 nm and weak shoulders near 218 nm with both spectra, consistent with highly disordered states with a small degree of β structure (Fig. 1*D*). Multimeric assembly triggered by neutralization at pH 7.0 or 8.0 causes a substantial change in the CD spectrum, shifting the strong minimum and shoulder, suggesting significant structural changes during assembly. Although it is difficult to assign precise proportions of specific structures from these data, the spectra are consistent with the presence of both α helices and β structures. Interestingly, the spectra of multimers at pH 7.0 and 8.0 are highly similar despite the substantial difference in their assembly sizes (R_H = 10 *versus* 20 nm, respectively). Acid-induced disassembly largely restores the CD spectrum to that of the disordered form, consistent with reversibility of reflectin conformation between the unassembled and assembled states.

Design of reflectin mutants

Previous work showed that the tunability of *D. opalescens* reflectins is regulated by a neurotransmitter-triggered signal transduction cascade culminating in phosphorylation and consequent progressive charge neutralization of the cationic reflectins, driving their progressive condensation and hierarchical assembly in a reversible and cyclable manner (6, 8, 10, 16). Plotting the distribution of electrostatic charge along the *D. opalescens* A1 sequence reveals a high degree of charge patterning across the reflectin linkers under both acidic and neutral conditions (*i.e.* conditions in which the histidines are either protonated or deprotonated, respectively) (Fig. 2*A*). These features are generally conserved across the reflectins found in diverse cephalopods (Fig. S2). We generated and analyzed a collection of *D. opalescens* reflectin A1 mutants to better analyze the effect of charge on condensation and assembly *in vitro* (Fig. 2*B*). A1 was chosen as the mutational platform based on its readily reproducible, tunable, and reversible assembly (16). All mutants were expressed in bacteria and purified by methods identical to those used for the WT, with no substantial differences from WT observed during purification. Purity of all proteins was closely similar to that of WT (Fig. S3) (16).

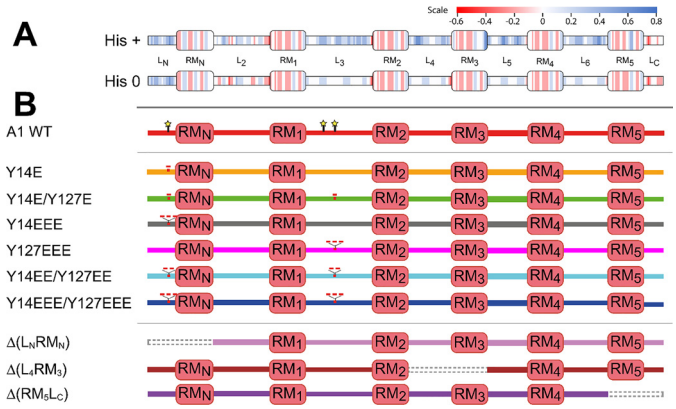

Figure 2. *A*, scaled net charge across *D. opalescens* reflectin A1 in the histidine-protonated (*top*) and histidine-deprotonated (*bottom*) states. Color is plotted from a centered five-residue moving window using the color key shown in the figure. *B*, *D. opalescens* reflectin A1 mutationally altered proteins investigated in this work. *Dotted gray lines* designate deleted segments in respective mutants. In both *A* and *B*, *boxes* indicate conserved domains, and *lines* indicate linkers.

Two classes of A1 mutants are investigated here. For the first class, we created a progressive series of phosphomimetic glutamate mutations at two previously identified sites of *in vivo* phosphorylation (Tyr-14 and Tyr-127) found to be associated with the activation of tunable iridescence in dorsal *D. opalescens* iridocytes (9). Mutants containing progressively increasing numbers of added glutamate residues allowed investigation of the incremental effects of charge neutralization on assembly, under conditions closely mimicking the effects of the physiological addition of two negative charges with each covalently attached phosphate. The second class of mutants consisted of deletions of conserved domain–linker segments from the N-terminal, central, or C-terminal regions of the protein. In *D. opalescens* A1, as in other reflectins (Figs. 2*A* and S2), the N-terminal linker is highly positively charged, whereas the more central linkers exhibit a lower but still significant net positive charge, and the C terminus itself is negatively charged. To maintain the linker/motif balance seen in WT A-type reflectins, all deletions removed paired linker and conserved domain segments. Due to the heterogenous charge distribution across reflectin A1, each deletion therefore uniquely modified the overall charge distribution of reflectin A1.

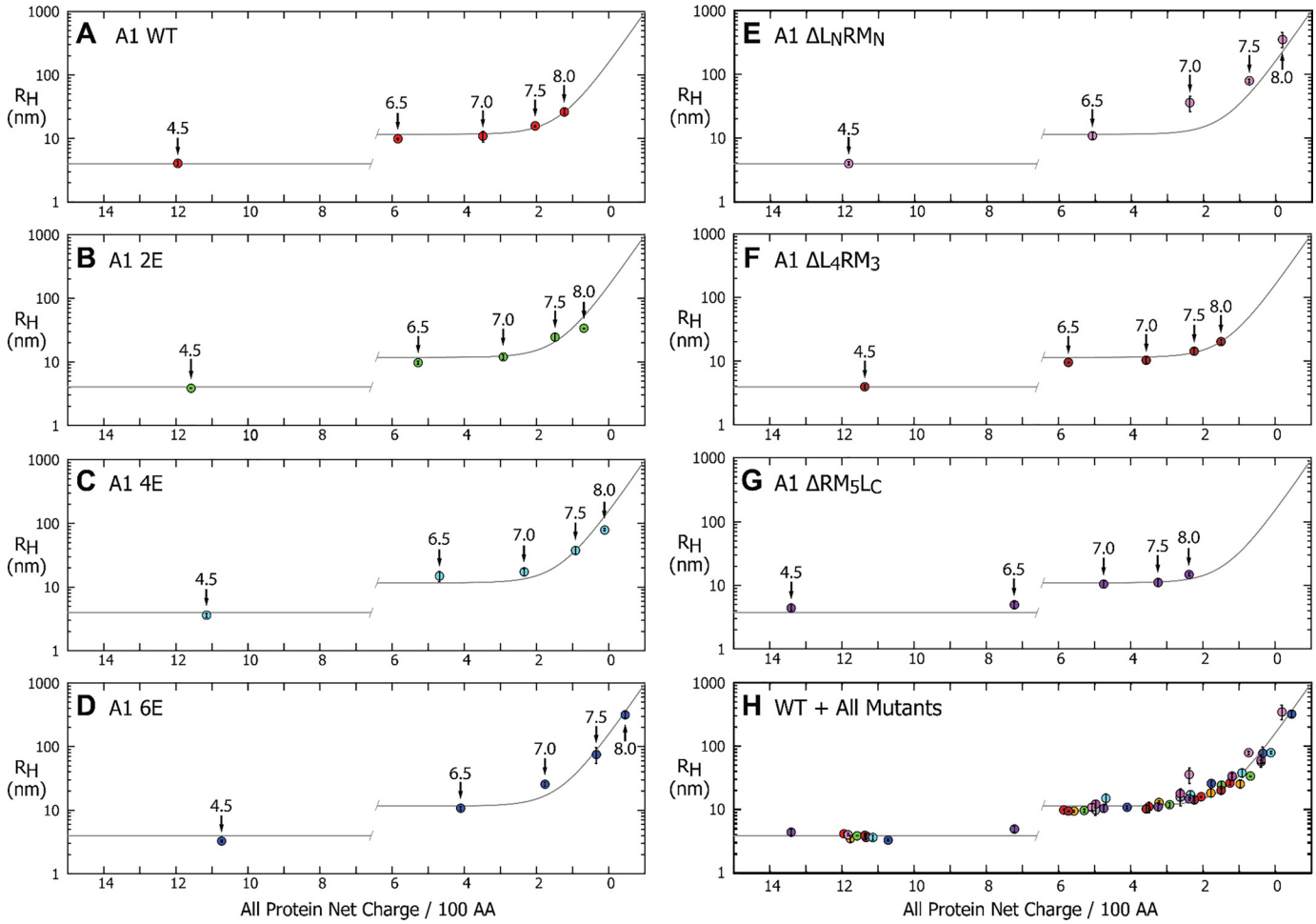

Figure 3. *A–H*, experimentally determined R_H measured by DLS *versus* calculated net charge density for A1 WT (*A*), selected A1 phosphomimetic mutants (*B–D*), A1 (conserved domain–linker)-deletion mutants (*E–G*). *H*, data for WT and all mutants collected on a single graph. pH at each data point is labeled with *arrows* in panels. The discontinuous *gray line* is the single-exponential least-squares fit of all A1 data for the multimers and is plotted as flat for the net charge density range corresponding to monomers. The position of discontinuity between monomeric and multimeric states is estimated. Representative DLS intensity and volume data are shown in Fig. S4; DLS size data against pH for all mutants are shown in Fig. S5. Sizes are plotted as a function of net charge density for each entire reflectin protein as calculated from Figs. S6 and described in the text. Each data point is the average of three replicate assembly measurements where each assembly measurement is an average of eight individual DLS measurements taken over the course of ~20 min immediately after sample preparation. *Error bars* signify ±1 S.D. between technical replicates.

Assembly behavior of reflectin mutants

We analyzed the pH-dependent assembly behavior of A1 WT and mutationally altered derivatives by DLS (Figs. 3, 4, S4, and S5), TEM, and atomic force microscopy (AFM) (Fig. 5). Reliable interpretation of DLS volume distributions and R_H values requires particles to be spherical, a requirement that is justified by the TEM and AFM imaging of the WT and mutant reflectin assemblies presented below and previously (16). Analyses by DLS (Fig. S4, *A* and *B*), TEM, and AFM show that WT reflectin A1 and the phosphomimetic (glutamate addition) and deletion mutants all form spherical assemblies of low polydispersity that are morphologically similar to those previously observed for WT (16). Also, like WT, assemblies of the reflectin mutants with R_H <100 formed and stabilized rapidly (within seconds or less), whereas larger assembles with R_H >100 nm were seen by DLS to exhibit some continuous slow growth (Fig. S4*C*). After their initial rapid growth, assemblies were relatively stable with time (growing no more than ~5–10% over several days at 25 °C), although particles with R_H >100 nm were observed to settle after ~30 min and could not usually be recovered by resuspension. Sizes measured by DLS were reproducible, with standard deviations between experimental replicates generally <10% when R_H was ≤100 nm, although larger standard deviations between replicates (up to 49%) were observed for large particle sizes ($R_H \gg 100$ nm).

Significantly, reductions in reflectin's net charge through mutagenesis, mimicking the effects of neurotransmitter-activated phosphorylation *in vivo*, resulted in large, systematic, and highly reproducible effects on the size of neutralization-induced assemblies. Mutationally altered reflectins with increasing numbers of additional glutamates formed progressively larger assemblies of well-defined size upon neutralization under identical conditions of pH, with this effect being enhanced at progressively higher pH (Figs. 3, *A–D*, and S5*A*). A single-site single glutamate mutant, A1 Y14E, assembled to sizes in the range of A1 WT, showing that abolition of the native tyrosine does not significantly perturb assembly (A1 Y127E also assembled similarly to A1 WT; data not shown). Further addition of negatively charged glutamates to A1 nonlinearly increased assembly size under identical pH conditions, with the

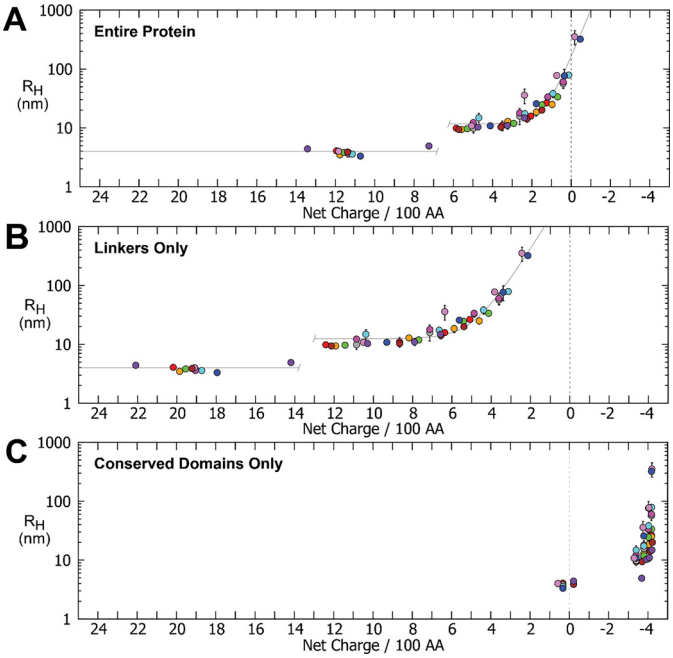

Figure 4. Experimentally measured R_H *versus* net charge density calculated for each entire protein or its conserved domains or linkers for A1 WT and mutants at different pH values. Colors correspond to specific mutants as in Figs. 2 and 3. Each data point is the average of three replicate assembly measurements where each assembly measurement is an average of eight individual DLS measurements of a sample, measured continuously, immediately after assembly. *Error bars* signify ±1 S.D. between averages of replicates. The *gray lines* are exponential fits to all A1 multimer data as in Fig. 3. *A*, R_H as a function of net charge density calculated for the entire A1 WT and mutant proteins (data from Fig. 3 are replotted for this comparison). *B*, R_H as a function of net charge density calculated only for the linkers of A1 WT and mutants. *C*, R_H as a function of net charge density calculated only for the conserved domains (both RM_N and $RM_{\#}$s) of A1 WT and mutants. *AA*, amino acids.

effects of mutational neutralization producing exponentially greater effects as pH is increased. Interestingly, both single-site triple glutamate mutants, A1 Y14EEE and A1 Y127EEE, exhibited similarly increasing sizes across the entire range of increasing pH tested, with those sizes being intermediate to those of the double A1 Y14E/Y127E mutant (with a total of two glutamates added) and those of the A1 Y14EE/Y127EE mutant (with a total of four glutamates added), indicating a relative insensitivity to the precise location of the added negative charges. A1 Y14EEE/Y127EEE, being maximally neutralized of these glutamate mutants, resulted in the largest assemblies, with well-defined sizes up to an R_H of ≈350 nm. All glutamate mutant assemblies were reversible by acidification with 15 mM acetic acid, pH 4.5, as previously observed for A1 WT (16).

Deletions of conserved domain–linker pair deletions also yielded reproducible effects on assembly size upon neutralization (Figs. 3, *E–G*, and S5*B*). An N-terminal conserved domain–linker pair deletion (A1 $\Delta L_N RM_N$) formed particles similar in size to the maximally neutralized phosphomimetic A1 Y14EEE/Y127EEE, whereas middle and C-terminal conserved domain–linker pair deletions (A1 $\Delta L_4 RM_3$ and $\Delta RM_5 L_C$, respectively) assembled to slightly decreased sizes relative to WT. Notably, A1 $\Delta RM_5 L_C$ formed R_H ≈4-nm particles at pH 6.5 of likely monomeric form (Fig. 3*G*), similar to pH 4.5 conditions for WT and other mutants and unlike the multimers normally observed at this pH. Interestingly, deletion mutants showed inconsistent reversal upon acidification with 15 mM acetic acid, pH 4.5, with oligomers only being intermittently detectable by DLS (data not shown).

Net charge density precisely determines reflectin assembly size

Strikingly, we found that the 30-min-assembly sizes of the WT and all mutants from both classes fall on the same plot when graphed as a function of the net charge density calculated for each protein (Fig. 3, particularly *H*). Our calculation of net charge density assumed invariant side-chain pK_a values for N-terminal, C-terminal, and internal residues and 6.5 for the histidine pK_a (16, 22). Plots of calculated protein net charge and linear net charge density as a function of pH for A1 WT and the mutants discussed here are shown in Fig. S6, each analyzed for the entire reflectin protein (Fig. S6, *A–D*), the linkers only (Fig. S6, *E–H*), and the conserved domains only (Fig. S6, *I–L*). An apparent discontinuity is observable between monomeric A1 at high net charge densities (typically acidic, acetate-buffered conditions) and the formation of multimers of tunable size. This suggests that a discrete neutralization threshold must be passed to trigger *D. opalescens* reflectin assembly, after which the predictive exponential relationship between net charge density and reflectin assembly size is revealed.

Decomposition of these sequences into their component linker and domain segments shows that the net charge density of the conserved domains is poorly predictive of assembly size, whereas the net charge density of the linkers yields a predictive relationship with measured particle size quite similar to that observed for the entire protein (Fig. 4, *A–C*). We thus conclude that the neutralization-sensitive switch resides in the linkers, which function like a sensor in this respect. Because reflectin assembly size appears insensitive to both the location (see above) and the means of charge neutralization, whether through progressive glutamate addition or deletion or by pH titration, the switch therefore appears to be distributed among the spatially segregated linkers. These results, as illustrated in Figs. 3 and 4, all are consistent with the behavior of a charge-stabilized colloidal system.

Although increases in ionic strength have been shown to drive reflectin assembly (16), the analyses reported above all were conducted at low buffer concentrations (5 mM) to minimize changes in ionic strength with pH, and comparable results were observed with MES, MOPS, and Tris buffers, with pK_a values ranging from 6.1 to 8.0. Furthermore, the large progressive increase in assembly size of the reflectins observed as a function of added glutamate residues, all at the same value of pH, demonstrates that the assembly differences observed among the mutants at the same pH cannot be explained by any change in ionic strength but instead are well-predicted solely by each protein's net charge density (Figs. 4 and S4).

Characterization by EM, atomic force microscopy, and fluorescence

TEM analyses confirm that the reflectin A1 WT and mutants form assemblies of spheroidal morphology and relatively low polydispersity, with sizes measured by TEM agreeing well with those determined by DLS (Fig. 5, *A–E*). Similarity between A1

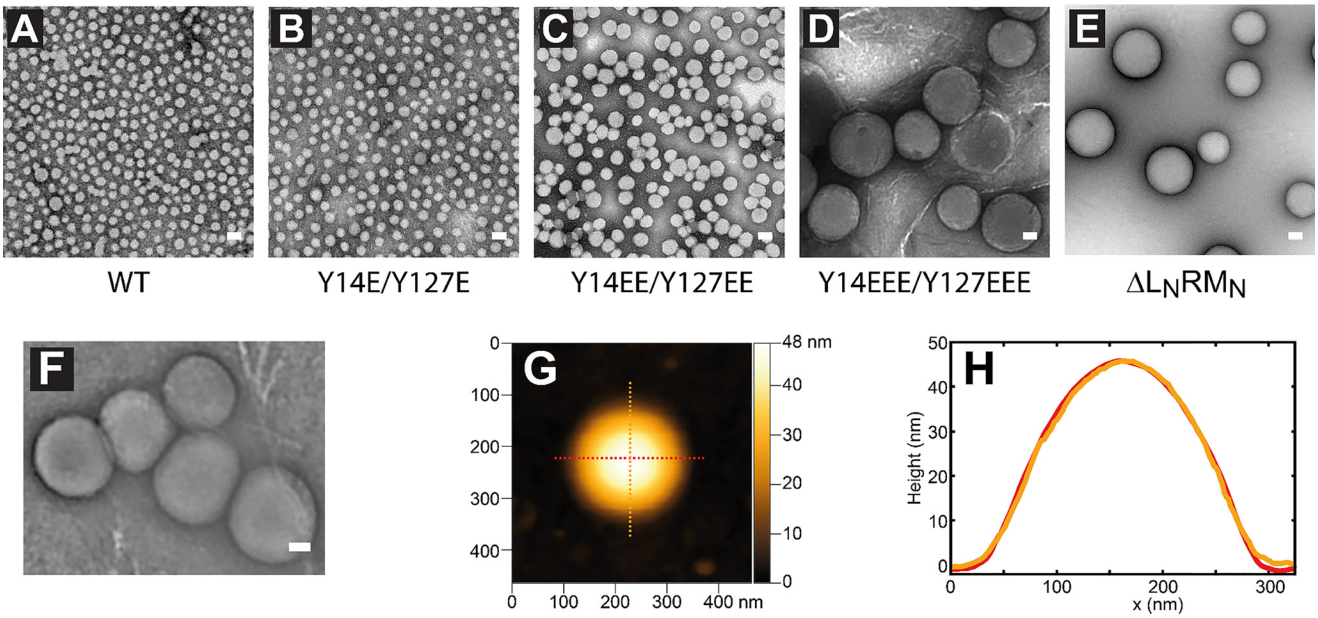

Figure 5. *A–E*, TEM images of A1 WT and glutamate mutants in 5 mM MOPS, pH 7. 5. *Scale bars*, 50 nm. All TEM images in *A–E* have not been postprocessed. Assemblies measured by DLS before application to the EM grids were as follows: *A*, A1 WT; DLS R_H = 16 nm; *B*, A1 Y14E/Y127E; DLS R_H = 22 nm; *C*, A1 Y14EE/Y127EE; DLS R_H = 31 nm; *D*, A1 Y14EEE/Y127EEE; DLS R_H = 98 nm; *E*, A1 $\Delta L_N RM_N$; DLS R_H = 77 nm. *F*, cluster of A1 Y14EEE/Y127EEE particles, demonstrating deformation. Scale bar, 50 nm. The image was processed using a digital bandpass filter to enhance contrast (53). *G*, atomic force microscope image of an A1 $\Delta L_N RM_N$ multimeric particle assembled in 5 mM MOPS, pH 7.5. *H*, height profiles of portions of the A1 $\Delta L_N RM_N$ particle shown in the previous panel as indicated.

WT and A1 Y14E/Y127E confirms that tyrosine mutagenesis itself does not generate aberrant assemblies. Particle size analysis from TEM of A1 WT and A1 Y14EEE/Y127EEE assemblies shows similar magnitudes of size variation (A1 WT polydispersity = 9%; A1 Y14EEE/Y127EEE polydispersity = 16%) (Fig. S7). Imaging of the N-terminal deletion $\Delta L_N RM_N$ shows that it also assembles to form spheres consistent in size with the results from DLS. Close correspondence in assembly sizes measured in the hydrated state by DLS and upon drying on TEM grids suggests that the assemblies are stable and likely to possess low water content and internal dynamics because they do not destructively shrink or collapse upon drying following application to the grid or exposure to vacuum in the electron microscope. Some larger assemblies, although appearing round in isolation, show distortions in morphology when packed into clusters, indicating that they are deformable and do not coalesce (Fig. 5*F*). Examination of air-dried reflectin particles by atomic force microscopy confirmed the highly symmetrical and smooth morphology of the reflectin assemblies (Fig. 5, *G* and *H*). Air-dried particles showed signs of flattening vertically with concomitant lateral expansion on the glass surface, demonstrating the same deformable nature observed by TEM for packed particles.

The spheroidal and highly smooth appearance of the assemblies, particularly marked for larger assemblies such A1 Y14EEE/Y127EEE and $\Delta L_N RM_N$, strongly suggests that a liquid-like phase transition occurs during assembly. However, the observed stability of these assemblies over time, their stability after drying, and the absence of any observed macroscopic phase separation as would result from coalescence all suggest that such a liquid-like phase possesses high interfacial energy and/or may rapidly solidify in a reversible manner, although the deformable viscoelastic behavior of the large particles indicates that they are not entirely solidified.

D. opalescens reflectin A1 is strongly UV-fluorescent, as it contains 10 tryptophans, seven of which are in highly conserved positions. Tryptophan fluorescence of the various phosphomimetic mutant nanoparticulate assemblies varied with charge neutralization–driven size in a manner essentially indistinguishable from that of WT (Fig. S8; fluorescence of A1 WT was reported previously (16)), demonstrating that the substitution mutations produced no significant changes in internal structure observable by this method.

Differences in net charge density explain differences between A1 and A2

Extending our application of net charge density beyond A1, we discovered that our previously reported observation of differences between the assembly behaviors of reflectins A1 and A2 can now be understood. TEM shows that neutralized A2 assemblies have morphologies similar to those found for A1 (Fig. S9A). However, despite an identical pI and >70% sequence identity with A1, A2 differed in response to addition of acetic acid after assembly, with A2 being nonreversible (16). Based on the experiments studying A1 assembly described above, we hypothesized that A2 assembly behavior can be readily understood to result from its lower percent histidine content; upon acidification, an insufficient number of histidines are protonated to sufficiently disrupt the assembly by coulombic repulsion (Fig. 6*A*). To test this hypothesis, we designed *D. opalescens* A2 mutants that contained an additional five (named A2+5H) and 10 (A2+10H) histidines spatially distributed among the linkers (Figs. 6, *A–C*, and S9*B*). We then compared the assembly and disassembly behavior of these muta-

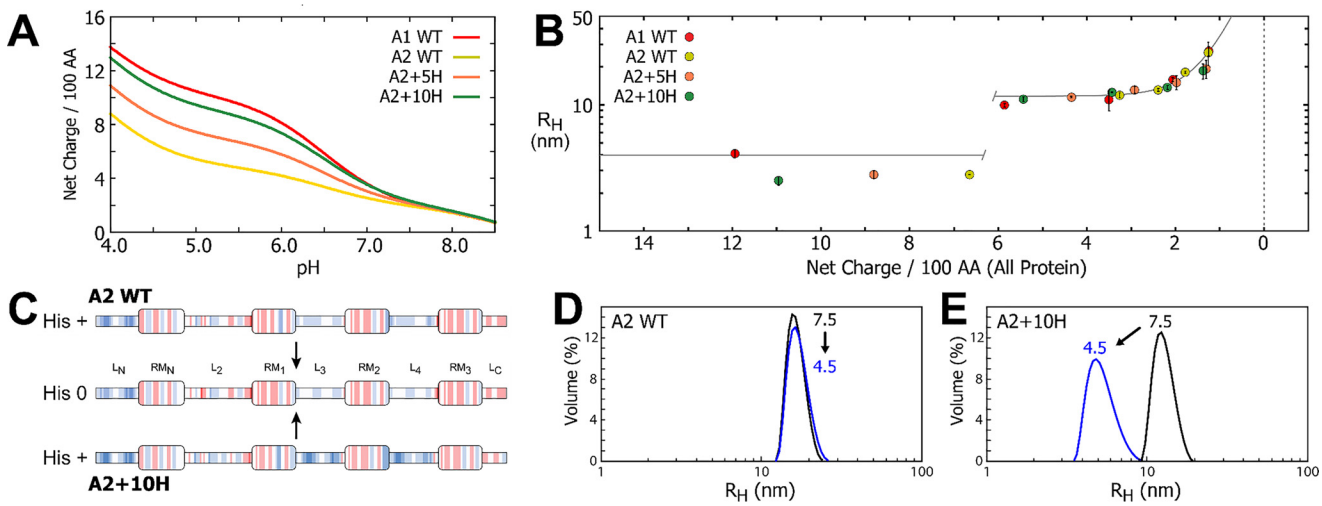

Figure 6. Comparison of *D. opalescens* reflectin A2 with A1 WT and mutants and results for A2 histidine charge mutants. *A*, net charge density calculated as a function of pH for A1 WT, A2 WT, and A2 mutants. Each data point is the average of three replicate assembly measurements where each assembly measurement is an average of eight individual DLS measurements of a sample, measured continuously, immediately after assembly. *Error bars* signify ±1 S.D. between replicate averages. *B*, experimental R_H as a function of calculated net charge density of 9 μM A1 WT, A2 WT, A2+5H, and A2+10H under the same pH range and conditions as A1 WT and mutants discussed earlier. The *gray line* is a single-exponential fit to all A1 multimer data as in Figs. 3 and 4. *C*, comparison of charge distributions across A2 WT and A2+10H in histidine-protonated and histidine-uncharged states as described for Fig. 2*A*. Charge distributions of A2 WT, A2+5H, and A2+10H are indistinguishable in the neutralized state. *D* and *E*, DLS volume distributions showing nonreversibility of A2 WT (*D*) and reversibility of A2+10H (*E*). *AA*, amino acids.

tionally altered reflectins with that of A2 WT as a function of pH (Fig. 6, *B* and *D*). Both histidine mutants of A2 assembled to similar sizes as WT, as expected based on net charge density, and followed the same net charge density curve derived from the A1 multimers (Fig. 6*B*), supporting the conclusion that self-limitation of assembly size is determined by spatially distributed electrostatic interactions across the reflectin chain. Notably, the same net charge density dependence was observed for A1 and A2 despite their differences in length, with A1 consisting of 350 amino acid residues and A2 having 230. DLS intensity and volume distributions for A2+5H and A2+10H did not differ from those of A2 WT (shown previously (16)), showing that these mutants are not more prone to form larger aggregates than A2 WT and suggesting that variations in histidine composition do not alter the nature of reflectin assembly. This insensitivity is consistent with the broadly similar assembly behavior of WT A1 and A2 despite their differences in histidine content (9 and 3% histidine, respectively). Recent work has shown that compounds including aromatic rings (generally in the mM concentration range), such as imidazole, drive assembly of *Sepia officinalis* reflectin 2, presumably through formation of new $\pi-\pi$ bonds (21). However, those results had been obtained with reflectin from a different species, analyzed in the presence of the detergent SDS or as an N-terminal fusion of a reflectin fragment with a significantly larger maltose-binding protein. In contrast, our results show that, in the absence of SDS, moderate variations in reflectin sequence histidine content are well-tolerated, consistent with the variation seen among reflectin sequences among different species. However, despite their similarities in assembly behavior, the histidine mutants of A2 differed significantly from the WT in their disassembly upon acidification. Although A2 WT was not reversible as measured by DLS in >90% of measurements, the A2+10H mutant protein was reversible in >90% of measurements (Fig. 6, *D* and *E*), forming R_H ≈12-nm particles as measured by DLS. Interestingly, A2+5H showed variable reversing behavior, being largely reversible at pH ≤7.0 and irreversible at pH ≥7.0, consistent with A2+5H possessing a net charge density near the charge threshold for assembly/disassembly.

Discussion

Reflectins assemble within cephalopod cells to form complex condensed nanostructures of high refractive index that produce diverse biophotonic effects (5–9, 14, 16). In most cephalopods, these structures are static, arising early during cellular development and remaining fixed for the lifetime of the cell (23). However, within the loliginid squids, some iridocyte (iridescent/narrowband) and leucophore (broadband) cells demonstrate tunable, cyclable, acetylcholine-dependent reflectivity (6, 24). Ultrastructural and immunohistochemical characterization of iridocyte Bragg lamellae shows that unactivated tunable iridocytes are filled with a heterogenous network of small reflectin nanoparticles (~10–20 nm in diameter) and nanofibers (7, 9, 11). Upon exposure to acetylcholine, phosphorylation of reflectin A1 and A2 drives neutralization and concomitant condensation and assembly, resulting in expulsion of water from the membrane-bounded Bragg lamellae, thus increasing the intralamellar protein density while shrinking the thickness and spacing of the lamellae. These physical changes increase the refractive index contrast between the reflectin-containing lamellae and the interspersed extracellular medium to activate reflectance while simultaneously tuning the reflected color (6, 8, 9, 24). Inspired by this unique biological function, studies have investigated the assembly and resulting optical behavior of purified recombinant reflectin and reflectin-based peptides. Purified reflectins and their peptides have been processed into a variety of optically active materials, including thin films, gratings, and fibers (18, 25). These thin films have optical properties that are reversibly sensitive to both hydration and pH (18–20, 25–28). In a nonoptical context, reflectin-based thin films have

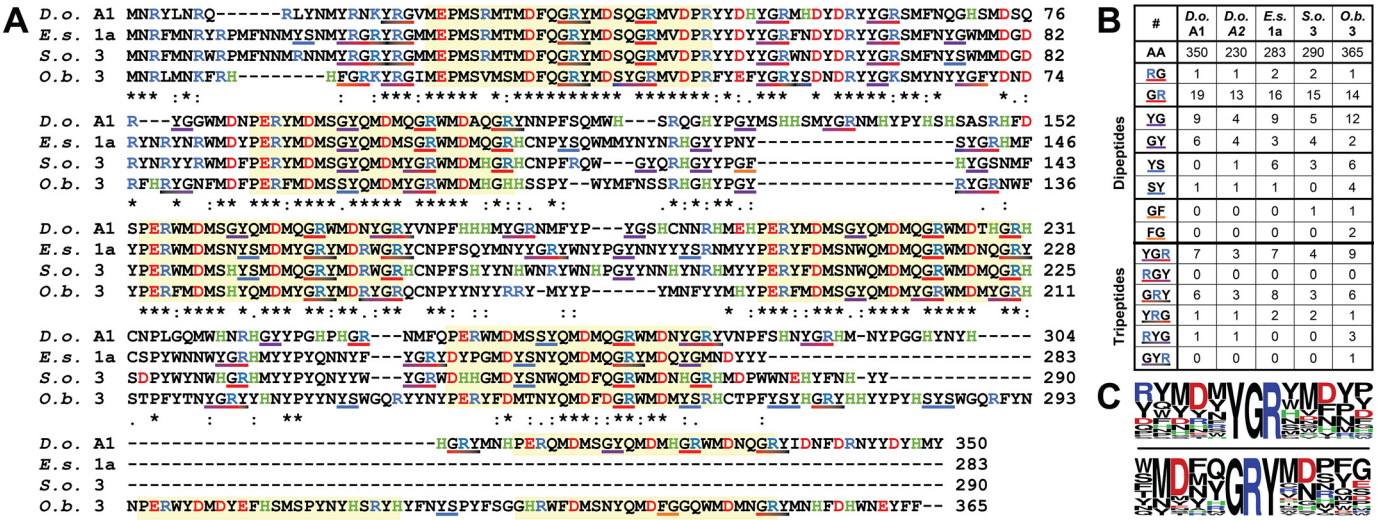

#	D.o. A1	D.o. A2	E.s. 1a	S.o. 3	O.b. 3
AA	350	230	283	290	365
RG	1	1	2	2	1
GR	19	13	16	15	14
YG	9	4	9	5	12
GY	6	4	3	4	2
YS	0	1	6	3	6
SY	1	1	1	0	4
GF	0	0	0	1	1
FG	0	0	0	0	2
YGR	7	3	7	4	9
RGY	0	0	0	0	0
GRY	6	3	8	3	6
YRG	1	1	2	2	1
RYG	1	1	0	0	3
GYR	0	0	0	0	1

Dipeptides

Tripeptides

Figure 7. Analysis of di- and tripeptides associated with liquid–liquid phase segregation in representative reflectin proteins. *A*, alignment of *D. opalescens* (*D. o.*) (squid) reflectin A1 (GenBank™ accession number KF661517.1), *Euprymna scolopes* (*E. s.*) (squid) reflectin 1a (AY294649.1), *Octopus bimaculoides* (*O. b.*) (octopus) reflectin 3 (KOF78298.1), and *S. officinalis* (*S. o.*) (cuttlefish) reflectin 3 (CCI88213.1). Conserved reflectin domains are highlighted in *yellow*. LLPS-associated di- (*solid colors*) and tripeptides (*gradient colors*) are *underlined* as labeled in the *table*. Alignment was performed using Clustal Omega (55). *B*, numbers of LLPS-associated di- and tripeptides in selected reflectin proteins. *C*, sequence logos of regions surrounding YGR (*upper*) and GRY (*lower*) tripeptides seen in reflectins listed in *B* (56). *AA*, amino acids.

also been investigated as proton conductors and transistors as well as substrates for neural cell growth (29–32).

Starting from the highly disordered, H_2O-solubilized reflectin monomers, we found that progressive neutralization drives the assembly of a collection of *D. opalescens* A1 WT and mutationally altered variants, with the resulting multimeric assembly sizes being predictively tuned by the normalized net charge density of the spatially distributed, cationic linkers that act as an electrostatic sensor and switch. Assembly size is indifferent to the mode of charge neutralization (whether by genetic alteration, pH titration, or both, acting as surrogates of phosphorylation *in vivo*) and indifferent to the location of the cationic linkers remaining after deletion. TEM analyses reveal the multimeric assemblies to be spherical with small size variation. Assembly sizes measured by DLS and TEM agree closely with each other as well as with small angle X-ray scattering measurements of assemblies.[3] The consistency of spherical morphology and internal structure (indicated by tryptophan fluorescence) between WT and mutant reflectins indicates that the assembly of these mutant reflectins is not the result of aberrant or off-pathway aggregation but lies on the common continuum, as also suggested by the colinearity of data for the mutants and WT (Figs. 3 and 4). Coulombic repulsion presumably contributes to maintenance of the positively charged reflectins in an extended, disordered, and monomeric state, with progressive neutralization progressively overcoming that repulsion to permit condensation and assembly. The strong predictive relationship observed between the net charge density of the cationic linkers and reflectin's final assembly size indicates that electrostatic interactions in some way limit that size.

To undergo assembly, the disordered reflectin monomers must pass through a net charge neutralization threshold, at which point they form multimers exhibiting an apparently exponential relationship between assembly size and calculated net charge density. Size control of reflectin assembly, tuned by changes in histidine protonation within the pH range tested here, is governed by a spatially distributed switch spread across the reflectin linkers. This behavior is consistent with the location of the previously identified sites of *in vivo* phosphorylation, almost exclusively found within the cationic linkers (6, 9). The tunable and reversible assembly of the reflectin proteins resembles that of the intrinsically disordered amelogenin proteins, which have been observed to form monomers, oligomers, and larger nanoparticle multimers in a pH-controlled manner and for which oligomers are thought to serve as the building blocks for larger nanoparticles (33, 34). However, unlike the amelogenins, the reflectins form assemblies of tunable size with low polydispersity as a function of neutralization, suggesting that some aspects of the unique reflectin amino acid composition and sequence enable a finer degree of control and tunability.

Comparison of *D. opalescens* reflectin A1 with similarly sized representative reflectins from other cephalopods that have nontunable iridescence shows that the N-terminal half of the reflectins generally possesses greater conservation (~50%) than the C-terminal half (~30%) (Fig. 7*A*). Interestingly, the N-terminal region, L_N, possesses a well-conserved, strongly cationic character across all reflectins, being composed of ~19–26% arginine compared with 11–12% arginine in the reflectins' full sequences overall. The conserved cationic character of L_N, combined with our finding that the $\Delta L_N RM_N$ mutant forms large assemblies, suggests that this linker may promote solubility during reflectin translation by inhibiting potential off-pathway aggregation through charge repulsion. Overall, our results show that linker electrostatics control reflectin condensation and assembly, consistent with the *in vivo* regulation by phosphorylation. In these respects, the behavior of the reflectins is consistent with that of a charge-stabilized colloidal system, although additional complexity is apparent (35, 36).

[3] R. Levenson, P. Kohl, Y. Li, and D. Morse, unpublished data.

Reflectins are highly enriched in conserved arginine (11%), tyrosine (20%), and methionine (15%) residues and relatively deficient in lysines and residues with simple aliphatic side chains (<1%). Enrichment in these residues is associated with the liquid–liquid phase segregation (LLPS) of multivalent, intrinsically disordered proteins that form biomolecular condensates, also known as coacervates, mediated through the formation of extensive webbed networks of relatively weak, short-range cation–π, sulfur–π, and π–π associative interactions (37–39). Arginine and tyrosine residues, abundant in the reflectins, have been recognized as particularly strong drivers of protein LLPS, often paired with glycine or serine (39–43). An analysis of reflectin proteins from diverse cephalopods for di- and tripeptide sequence motifs associated with LLPS reveals a high occurrence of sequentially biased Arg-Gly, Tyr-Gly, and Tyr-Ser dipeptide sequences (Fig. 7, *A* and *B*), comprising ~20% of the entire reflectin sequence (40, 42–44). Notably, these dipeptide motifs are substantially clustered together to from a significant number of Tyr-Gly-Arg and Gly-Arg-Tyr tripeptides (Fig. 7, *A*–*C*). Given their high frequency and conservation in the reflectins, we suggest that these di- and tripeptides may play a critical role in driving reflectin LLPS. Based on the distribution of these associative peptide motifs throughout the reflectins, it is likely that both the conserved domains and the linkers robustly and directly participate in noncovalent bond formation during neutralization-triggered condensation.

Although the sphericity of the large reflectin A1 assemblies formed *in vitro* also is consistent with the suggestion that a transient phase-segregated liquid state may be formed upon sufficient charge neutralization and subsequent formation of reflectin condensates, the stability of reflectin assemblies and absence of coalescence and macroscopic phase separation (as observed by DLS and microscopy) indicate that these particles do not persist in this state of low interfacial energy but apparently undergo rapid dynamic arrest of further assembly, preventing further coalescence or phase separation (16, 38, 45). Such arrest (variously also described as hardening, gelation, solidification, or vitrification) of LLPS condensates has been widely observed in other systems and in several cases is associated with pathology; in some instances, it is accompanied by deformations of the initially spherical assemblies (38, 45). We have observed such gel-like deformation with compaction of reflectin assemblies (Fig. 5*F*). Formally, dynamic arrest of assembly is determined by the balance of short-range (weak) attractive forces and long-range (strong) repulsive forces, as well-understood for many colloidal systems. In the case of reflectin assembly, the weak attractive forces potentially include a combination of hydrogen and hydrophobic bonding, β-stacking, coil–coil interactions, cation–π, sulfur–π, π–π, van der Waals and other forms of noncovalent bonding, whereas coulombic repulsion, which we have experimentally tuned here by pH titration of histidine and by mutation, likely comprises the dominant counteracting repulsive interaction.

It is interesting that it is the dynamic arrest of reflectin assembly that is responsible for the precise and finely tunable relationship between the extent of charge neutralization and the resulting size and number of reflectin assemblies. This dynamic arrest of neutralization-driven assembly is thus in turn responsible for the precise control of the colligatively triggered osmotic motor that proportionally drives the cyclable dehydration of the membrane-bounded subcellular Bragg lamellae containing the reflectins, proportionally and simultaneously increasing refractive index and shrinking the dimensions of the lamellae to tune the reflected light (8). The precise relationship between the extent of charge neutralization and size of reflectin assembly (with its reciprocal control of particle number concentration), followed by rapid dynamic arrest as described here, thus ensures a precise calibration between the triggering neuronal signal (and its consequent phosphorylation of reflectin) and the resulting change in color in squid skin. The reflectin's unique sequence composition, rich in aromatic residues and sulfur-containing methionine, apparently enables a further synergistic enhancement of this photonic tuning, providing the reflectins with one of the highest known incremental refractive indices (dn/dc) and thus allowing the reflectins to generate higher-refractive-index contrast with the extracellular fluid in the physiological Bragg reflectors while also driving their tunable assembly (10, 46).

Genomic sequencing of cephalopods is now revealing an ever-increasing family of unique reflectin sequences, suggesting that a rich network of inter-reflectin interactions may occur within cephalopod Bragg reflectors (5, 10, 23, 47). The results reported here highlight the unique properties of the tunable reflectins that enable them to function as a finely tuned molecular machine that precisely regulates an osmotic motor to mechanically tune the color and intensity of light reflected from intracellular nanophotonic structures. Extending the reflectin-based thin-film applications described above (18, 19, 25–28), the unique structure–function relationships of the highly evolved tunable reflectins may provide inspiration and guidance for future classes of tunably reconfigurable optical and other materials, open further possibilities for exploration of the design principles underlying reflectin assembly, and suggest new pathways toward the rational design of tunable assembly (48, 49).

Experimental procedures

Bioinformatics and sequence net charge calculations

Intrinsic disorder in the *D. opalescens* reflectins was predicted using the web-based servers FoldIndex (50), PONDR-FIT (51), and MetaDisorder (52) using default settings.

Reflectin mutagenesis, expression, purification, solubilization, and buffer preparation

Recombinant *D. opalescens* reflectin A1 mutants were produced by mutagenesis, using standard techniques, of a non-affinity-tagged, codon-optimized reflectin A1 WT construct cloned into a pJ411 plasmid (purchased from ATUM, San Francisco, CA) (7, 16). All mutants were confirmed by DNA sequencing. Codon-optimized DNA sequences encoding the A2+5H/A2+10H mutants within the same pJ411 plasmid were also purchased from ATUM. Protein expression and purification were performed as reported previously (16). All proteins were expressed in Rosetta 2 (DE3) *Escherichia coli* cells grown at 37 °C in liter LB cultures from freshly plated transformants in the presence of 50 mg/ml kanamycin and 37 mg/ml chloram-

phenicol. Expression was induced at A_{600} ~0.6 and allowed to proceed for ~6 h at 37 °C, at which point cells were pelleted by centrifugation and frozen at −80 °C until ready for use.

All reflectin proteins were expressed as inclusion bodies, similarly to WT, with roughly similar yields as judged by comparison on SDS-polyacrylamide gels. Reflectin inclusion bodies were purified from cell pellets with BugBuster medium (Novagen, Inc., Madison, WI) as directed by the manufacturer. Inclusion bodies were solubilized in 5% acetic acid, 8 M urea, 6 M guanidinium HCl followed by dialysis against 5% acetic acid, 8 M urea to remove guanidinium. Proteins were purified by ion exchange over a HiTrap XL (GE Healthcare) cation-exchange column and eluted with a gradient of 5% acetic acid, 6 M guanidinium. Fractions containing reflectin were collected; diluted in 5% acetic acid, 8 M urea to lower guanidinium concentration; loaded onto a Mono S GL column (GE Healthcare); and then eluted with a step gradient of 5% acetic acid, 6 M guanidinium. Eluted reflectin was concentrated, loaded onto an HPLC reverse-phase C_{10} column equilibrated with 0.1% trifluoroacetic acid (TFA) in H_2O, and then eluted over a gradient of 95% acetonitrile, 0.1% TFA. Fractions were then lyophilized and stored in a −80 °C freezer until solubilization. Purity was assessed on 10% Tris acetate SDS-polyacrylamide gels (Life Technologies). Purity of all proteins was the same as described previously (16).

Protein solubilization and neutralization assay

Lyophilized protein was solubilized in 0.22-μm-filtered H_2O. Protein concentration was determined by measuring absorbance at 280 nm using calculated extinction coefficients for each protein sequence. All freshly solubilized samples were diluted to 81 μM for use as stock solutions and stored at 4 °C between uses. To perform the neutralization assay, all protein stocks, buffers, and water were filtered upon preparation and centrifuged at 18,000 × *g* for 10 min promptly before use and equilibrated to room temperature. Protein stock solution was diluted in prepared buffer solution to make final concentrations of 9 μM protein in 5 mM buffer. Sizes of reflectins are sensitive to buffer concentration, with higher buffer concentration leading to larger multimeric assemblies as a result of electrostatic charge screening; however, trends at higher buffer concentrations are consistent with those shown here. To determine reversibility of assembly, 250 mM sodium acetate, pH 4.5 buffer was rapidly added and mixed to a final concentration of 15 mM.

Dynamic light scattering

DLS analysis was performed on a Malvern Zetasizer Nano ZS (Worcestershire, UK). All measurements were performed with pre-equilibrated 40-μl samples at 25 °C. Samples were measured continuously, immediately after assembly, generally for a minimum of 20 min to ensure sample equilibration and stability (16). All reflectin assembly size measurements were replicated three times, with each independent assembly sample receiving at least three DLS measurements per replicate.

To evaluate the effects of incremental additions of reflectin at a given pH, increments of 1.25 μl of 81 μM H_2O-solubilized A1 WT aliquots were added to 40 μl of starting neutralizing buffer, 5 mM MOPS, pH 7.5, within the DLS cuvette. Samples were measured immediately and continuously after addition of protein for ≥10 min, after which the next aliquot was added and measured.

Circular dichroism

All samples were measured on a Jasco J-1500 CD spectrophotometer using a 0.2-mm-pathlength demountable cuvette (Starna Cells, Inc., Atascadero, CA) at 25 °C. Reflectin monomer concentration in all experiments was 6 μM. Data shown are the averages of a minimum of four scans. For all data shown, high tension values were always less than 480 V.

Transmission EM

All reflectin assemblies analyzed were prepared from 9 μM reflectin in 5 mM MOPS, pH 7.5 buffer and measured by DLS before application to grids (16). 400-mesh carbon-coated grids (Electron Microscopy Sciences, Hatfield, PA) were first treated by glow discharge for 30 s, and then 5 μl of freshly prepared sample was applied for 2 min before removal by wicking with filter paper. Samples were negatively stained three times with 20 μl of freshly filtered 1.5% uranyl acetate for 20 s followed by immediate wicking. Samples were visualized with an FEI Tecnai G2 Sphere microscope at 200 kV. TEM images were processed in ImageJ 1.50i (53).

Atomic force microscopy

Assembled reflectin particles were applied for 30 s onto cleaned glass slides before removal of buffer by wicking with filter paper. Negative controls with only buffer applied did not reveal any comparable particles. Reflectin particles were analyzed in tapping mode on an MFP-3D atomic force microscope (Asylum Research, Santa Barbara, CA) with SSS-NCHR-10 high aspect ratio tips (Asylum Research). Data were processed using Gwyddion.

Fluorescence

Samples were analyzed on a Cary Eclipse spectrophotometer (Varian, Inc., Palo Alto, CA) (16). 200 μl of 9 μM samples was freshly prepared by neutralization assay before analysis. The experiment was performed at room temperature. Excitation and emission slits were 5 nm wide for all measurements.

Author contributions—R. L. and D. E. M. conceptualization; R. L. data curation; R. L. and D. E. M. supervision; R. L., C. B., C. S., J. S., C. A., and B. M. investigation; R. L. methodology; R. L. and D. E. M. writing-original draft; R. L. and D. E. M. writing-review and editing; D. E. M. resources; D. E. M. funding acquisition; D. E. M. project administration.

Acknowledgments—We thank Cristophe A. Monnier for assistance with AFM measurements. Use of the University of California, Santa Barbara, Materials Research Laboratory Shared Experimental Facilities, a member of the National Science Foundation-funded Materials Research Facilities Network, was supported by the Materials Research Science and Engineering Center Program of the National Science Foundation under Materials Research Award 1121053. We are grateful to Youli Li for insightful discussions.

References

1. Hanlon, R. (2007) Cephalopod dynamic camouflage. *Curr. Biol.* **17,** R400–R404 CrossRef Medline
2. Hanlon, R. T., Chiao, C.-C., Mäthger, L. M., Barbosa, A., Buresch, K. C., and Chubb, C. (2009) Cephalopod dynamic camouflage: bridging the continuum between background matching and disruptive coloration. *Philos. Trans. R. Soc. Lond. B Biol. Sci.* **364,** 429–437 CrossRef Medline
3. Kreit, E., Mäthger, L. M., Hanlon, R. T., Dennis, P. B., Naik, R. R., Forsythe, E., and Heikenfeld, J. (2013) Biological versus electronic adaptive coloration: how can one inform the other? *J. R. Soc. Interface* **10,** 20120601 CrossRef Medline
4. Mäthger, L. M., Senft, S. L., Gao, M., Karaveli, S., Bell, G. R. R., Zia, R., Kuzirian, A. M., Dennis, P. B., Crookes-Goodson, W. J., Naik, R. R., Kattawar, G. W., and Hanlon, R. T. (2013) Bright white scattering from protein spheres in color changing, flexible cuttlefish skin. *Adv. Funct. Mater.* **23,** 3980–3989 CrossRef
5. Crookes, W. J., Ding, L.-L., Huang, Q. L., Kimbell, J. R., Horwitz, J., and McFall-Ngai, M. J. (2004) Reflectins: the unusual proteins of squid reflective tissues. *Science* **303,** 235–238 CrossRef Medline
6. Izumi, M., Sweeney, A. M., Demartini, D., Weaver, J. C., Powers, M. L., Tao, A., Silvas, T. V., Kramer, R. M., Crookes-Goodson, W. J., Mäthger, L. M., Naik, R. R., Hanlon, R. T., and Morse, D. E. (2010) Changes in reflectin protein phosphorylation are associated with dynamic iridescence in squid. *J. R. Soc. Interface* **7,** 549–560 CrossRef Medline
7. Tao, A. R., DeMartini, D. G., Izumi, M., Sweeney, A. M., Holt, A. L., and Morse, D. E. (2010) The role of protein assembly in dynamically tunable bio-optical tissues. *Biomaterials* **31,** 793–801 CrossRef Medline
8. DeMartini, D. G., Krogstad, D. V., and Morse, D. E. (2013) Membrane invaginations facilitate reversible water flux driving tunable iridescence in a dynamic biophotonic system. *Proc. Natl. Acad. Sci. U.S.A.* **110,** 2552–2556 CrossRef Medline
9. DeMartini, D. G., Izumi, M., Weaver, A. T., Pandolfi, E., and Morse, D. E. (2015) Structures, organization, and function of reflectin proteins in dynamically tunable reflective cells. *J. Biol. Chem.* **290,** 15238–15249 CrossRef Medline
10. Levenson, R., DeMartini, D. G., and Morse, D. E. (2017) Molecular mechanism of reflectin's tunable biophotonic control: opportunities and limitations for new optoelectronics. *APL Mater.* **5,** 104801 CrossRef
11. Cooper, K. M., Hanlon, R. T., and Budelmann, B. U. (1990) Physiological color change in squid iridophores. II. Ultrastructural mechanisms in *Lolliguncula brevis*. *Cell Tissue Res.* **259,** 15–24 CrossRef Medline
12. Cooper, K. M., and Hanlon, R. T. (1986) Correlation of iridescence with changes in iridophore platelet ultrastructure in the squid *Lolliguncula brevis*. *J. Exp. Biol.* **121,** 451–455 Medline
13. Ghoshal, A., Demartini, D. G., Eck, E., and Morse, D. E. (2013) Optical parameters of the tunable Bragg reflectors in squid. *J. R. Soc. Interface* **10,** 20130386 CrossRef Medline
14. Ghoshal, A., DeMartini, D. G., Eck, E., and Morse, D. E. (2014) Experimental determination of refractive index of condensed reflectin in squid iridocytes. *J. R. Soc. Interface* **11,** 20140106 CrossRef Medline
15. Vernon, R. M., Chong, P. A., Tsang, B., Kim, T. H., Bah, A., Farber, P., Lin, H., and Forman-Kay, J. D. (2018) π-π contacts are an overlooked protein feature relevant to phase separation. *eLife* **7,** e31486 CrossRef Medline
16. Levenson, R., Bracken, C., Bush, N., and Morse, D. E. (2016) Cyclable condensation and hierarchical assembly of metastable reflectin proteins, the drivers of tunable biophotonics. *J. Biol. Chem.* **291,** 4058–4068 CrossRef Medline
17. Uversky, V. N., Gillespie, J. R., and Fink, A. L. (2000) Why are "natively unfolded" proteins unstructured under physiologic conditions? *Proteins* **41,** 415–427 CrossRef Medline
18. Qin, G., Dennis, P. B., Zhang, Y., Hu, X., Bressner, J. E., Sun, Z., Crookes-Goodson, W. J., Naik, R. R., Omenetto, F. G., and Kaplan, D. L. (2013) Recombinant reflectin-based optical materials. *J. Polym. Sci. Part B Polym. Phys.* **51,** 254–264 CrossRef
19. Phan, L., Walkup, W. G., 4th, Ordinario, D. D., Karshalev, E., Jocson, J.-M., Burke, A. M., and Gorodetsky, A. A. (2013) Reconfigurable infrared camouflage coatings from a cephalopod protein. *Adv. Mater.* **25,** 5621–5625 CrossRef Medline
20. Naughton, K. L., Phan, L., Leung, E. M., Kautz, R., Lin, Q., Van Dyke, Y., Marmiroli, B., Sartori, B., Arvai, A., Li, S., Pique, M. E., Naeim, M., Kerr, J. P., Aquino, M. J., Roberts, V. A., *et al.* (2016) Self-assembly of the cephalopod protein reflectin. *Adv. Mater.* **28,** 8405–8412 CrossRef Medline
21. Guan, Z., Cai, T., Liu, Z., Dou, Y., Hu, X., Zhang, P., Sun, X., Li, H., Kuang, Y., Zhai, Q., Ruan, H., Li, X., Li, Z., Zhu, Q., Mai, J., *et al.* (2017) Origin of the reflectin gene and hierarchical assembly of its protein. *Curr. Biol.* **27,** 2833–2842.e6 CrossRef Medline
22. Thurlkill, R. L., Grimsley, G. R., Scholtz, J. M., and Pace, C. N. (2006) pK values of the ionizable groups of proteins. *Protein Sci.* **15,** 1214–1218 CrossRef Medline
23. Andouche, A., Bassaglia, Y., Baratte, S., and Bonnaud, L. (2013) Reflectin genes and development of iridophore patterns in *Sepia officinalis* embryos (Mollusca, Cephalopoda). *Dev. Dyn.* **242,** 560–571 CrossRef Medline
24. DeMartini, D. G., Ghoshal, A., Pandolfi, E., Weaver, A. T., Baum, M., and Morse, D. E. (2013) Dynamic biophotonics: female squid exhibit sexually dimorphic tunable leucophores and iridocytes. *J. Exp. Biol.* **216,** 3733–3741 CrossRef Medline
25. Kramer, R. M., Crookes-Goodson, W. J., and Naik, R. R. (2007) The self-organizing properties of squid reflectin protein. *Nat. Mater.* **6,** 533–538 CrossRef Medline
26. Phan, L., Ordinario, D. D., Karshalev, E., Iv, W. G. W., Shenk, M. A., and Gorodetsky, A. A. (2015) Infrared invisibility stickers inspired by cephalopods. *J. Mater. Chem. C.* **3,** 6493–6498 CrossRef
27. Phan, L., Kautz, R., Leung, E. M., Naughton, K. L., Van Dyke, Y., and Gorodetsky, A. A. (2016) Dynamic materials inspired by cephalopods. *Chem. Mater.* **28,** 6804–6816 CrossRef
28. Dennis, P. B., Singh, K. M., Vasudev, M. C., Naik, R. R., and Crookes-Goodson, W. J. (2017) Research update: a minimal region of squid reflectin for vapor-induced light scattering. *APL Mater.* **5,** 120701 CrossRef
29. Ordinario, D. D., Phan, L., Walkup, W. G., 4th, Jocson, J.-M., Karshalev, E., Hüsken, N., and Gorodetsky, A. A. (2014) Bulk protonic conductivity in a cephalopod structural protein. *Nat. Chem.* **6,** 596–602 CrossRef Medline
30. Ordinario, D. D., Phan, L., Iv, W. G. W., Dyke, Y. V., Leung, E. M., Nguyen, M., Smith, A. G., Kerr, J., Naeim, M., Kymissis, I., and Gorodetsky, A. A. (2016) Production and electrical characterization of the reflectin A2 isoform from *Doryteuthis* (*Loligo*) *pealeii*. *RSC Adv.* **6,** 57103–57107 CrossRef
31. Ordinario, D. D., Phan, L., Van Dyke, Y., Nguyen, T., Smith, A. G., Nguyen, M., Mofid, N. M., Dao, M. K., and Gorodetsky, A. A. (2016) Photochemical doping of protonic transistors from a cephalopod protein. *Chem. Mater.* **28,** 3703–3710 CrossRef
32. Phan, L., Kautz, R., Arulmoli, J., Kim, I. H., Le, D. T., Shenk, M. A., Pathak, M. M., Flanagan, L. A., Tombola, F., and Gorodetsky, A. A. (2016) Reflectin as a material for neural stem cell growth. *ACS Appl. Mater. Interfaces* **8,** 278–284 CrossRef Medline
33. Margolis, H. C., Beniash, E., and Fowler, C. E. (2006) Role of macromolecular assembly of enamel matrix proteins in enamel formation. *J. Dent. Res.* **85,** 775–793 CrossRef Medline
34. Bromley, K. M., Kiss, A. S., Lokappa, S. B., Lakshminarayanan, R., Fan, D., Ndao, M., Evans, J. S., and Moradian-Oldak, J. (2011) Dissecting amelogenin protein nanospheres. *J. Biol. Chem.* **286,** 34643–34653 CrossRef Medline
35. Klein, R., and von Grünberg, H. H. (2001) Charge-stabilized colloidal suspensions. Phase behavior and effects of confinement. *Pure Appl. Chem.* **73,** 1705–1719 CrossRef
36. Hierrezuelo, J., Sadeghpour, A., Szilagyi, I., Vaccaro, A., and Borkovec, M. (2010) Electrostatic stabilization of charged colloidal particles with adsorbed polyelectrolytes of opposite charge. *Langmuir* **26,** 15109–15111 CrossRef Medline
37. Brangwynne, C. P., Tompa, P., and Pappu, R. V. (2015) Polymer physics of intracellular phase transitions. *Nat. Phys.* **11,** 899–904 CrossRef
38. Shin, Y., and Brangwynne, C. P. (2017) Liquid phase condensation in cell physiology and disease. *Science* **357,** eaaf4382 CrossRef Medline

39. Banani, S. F., Lee, H. O., Hyman, A. A., and Rosen, M. K. (2017) Biomolecular condensates: organizers of cellular biochemistry. *Nat. Rev. Mol. Cell Biol.* **18,** 285–298 CrossRef Medline
40. Qamar, S., Wang, G., Randle, S. J., Ruggeri, F. S., Varela, J. A., Lin, J. Q., Phillips, E. C., Miyashita, A., Williams, D., Ströhl, F., Meadows, W., Ferry, R., Dardov, V. J., Tartaglia, G. G., Farrer, L. A., *et al.* (2018) FUS phase separation Is modulated by a molecular chaperone and methylation of arginine cation-π interactions. *Cell.* **173,** 720–734.e15 CrossRef Medline
41. Thandapani, P., O'Connor, T. R., Bailey, T. L., and Richard, S. (2013) Defining the RGG/RG motif. *Mol. Cell* **50,** 613–623 CrossRef Medline
42. Chong, P. A., Vernon, R. M., and Forman-Kay, J. D. (2018) RGG/RG motif regions in RNA binding and phase separation. *J. Mol. Biol.* **430,** 4650–4665 CrossRef Medline
43. Lin, Y., Currie, S. L., and Rosen, M. K. (2017) Intrinsically disordered sequences enable modulation of protein phase separation through distributed tyrosine motifs. *J. Biol. Chem.* **292,** 19110–19120 CrossRef Medline
44. Schmidt, H. B., and Görlich, D. (2015) Nup98 FG domains from diverse species spontaneously phase-separate into particles with nuclear pore-like permselectivity. *eLife* **4,** e04251 CrossRefMedline
45. Woodruff, J. B., Hyman, A. A., and Boke, E. (2018) Organization and function of non-dynamic biomolecular condensates. *Trends Biochem. Sci.* **43,** 81–94 CrossRef Medline
46. Zhao, H., Brown, P. H., and Schuck, P. (2011) On the distribution of protein refractive index increments. *Biophys. J.* **100,** 2309–2317 CrossRef Medline
47. Albertin, C. B., Simakov, O., Mitros, T., Wang, Z. Y., Pungor, J. R., Edsinger-Gonzales, E., Brenner, S., Ragsdale, C. W., and Rokhsar, D. S. (2015) The octopus genome and the evolution of cephalopod neural and morphological novelties. *Nature* **524,** 220–224 CrossRef Medline
48. Dzuricky, M., Roberts, S., and Chilkoti, A. (2018) Convergence of artificial protein polymers and intrinsically disordered proteins. *Biochemistry* **57,** 2405–2414 CrossRef Medline
49. Ruff, K. M., Roberts, S., Chilkoti, A., and Pappu, R. V. (2018) Advances in understanding stimulus-responsive phase behavior of intrinsically disordered protein polymers. *J. Mol. Biol.* **430,** 4619–4635 CrossRef Medline
50. Prilusky, J., Felder, C. E., Zeev-Ben-Mordehai, T., Rydberg, E. H., Man, O., Beckmann, J. S., Silman, I., and Sussman, J. L. (2005) FoldIndex©: a simple tool to predict whether a given protein sequence is intrinsically unfolded. *Bioinformatics* **21,** 3435–3438 CrossRef Medline
51. Xue, B., Dunbrack, R. L., Williams, R. W., Dunker, A. K., and Uversky, V. N. (2010) PONDR-FIT: a meta-predictor of intrinsically disordered amino acids. *Biochim. Biophys. Acta* **1804,** 996–1010 CrossRef Medline
52. Kozlowski, L. P., and Bujnicki, J. M. (2012) MetaDisorder: a meta-server for the prediction of intrinsic disorder in proteins. *BMC Bioinformatics* **13,** 111 CrossRef Medline
53. Schneider, C. A., Rasband, W. S., and Eliceiri, K. W. (2012) NIH Image to ImageJ: 25 years of image analysis. *Nat. Methods* **9,** 671–675 CrossRef Medline
54. Kyte, J., and Doolittle, R. F. (1982) A simple method for displaying the hydropathic character of a protein. *J. Mol. Biol.* **157,** 105–132 CrossRef Medline
55. Sievers, F., Wilm, A., Dineen, D., Gibson, T. J., Karplus, K., Li, W., Lopez, R., McWilliam, H., Remmert, M., Söding, J., Thompson, J. D., and Higgins, D. G. (2011) Fast, scalable generation of high-quality protein multiple sequence alignments using Clustal Omega. *Mol. Syst. Biol.* **7,** 539 CrossRef Medline
56. Crooks, G. E., Hon, G., Chandonia, J.-M., and Brenner, S. E. (2004) WebLogo: a sequence logo generator. *Genome Res.* **14,** 1188–1190 CrossRef Medline